



OPEN

DATA DESCRIPTOR

# Thermodynamic and transport properties of hydrogen containing streams

Aliakbar Hassanpouryouzband<sup>1</sup> <sup>✉</sup>, Edris Joonaki<sup>2</sup>, Katriona Edlmann<sup>1</sup> <sup>✉</sup>, Niklas Heinemann<sup>1</sup> & Jinhai Yang<sup>3</sup>

The use of hydrogen (H<sub>2</sub>) as a substitute for fossil fuel, which accounts for the majority of the world's energy, is environmentally the most benign option for the reduction of CO<sub>2</sub> emissions. This will require gigawatt-scale storage systems and as such, H<sub>2</sub> storage in porous rocks in the subsurface will be required. Accurate estimation of the thermodynamic and transport properties of H<sub>2</sub> mixed with other gases found within the storage system is therefore essential for the efficient design for the processes involved in this system chain. In this study, we used the established and regarded GERG-2008 Equation of State (EoS) and SuperTRAPP model to predict the thermo-physical properties of H<sub>2</sub> mixed with CH<sub>4</sub>, N<sub>2</sub>, CO<sub>2</sub>, and a typical natural gas from the North-Sea. The data covers a wide range of mole fraction of H<sub>2</sub> (10–90 Mole%), pressures (0.01–100 MPa), and temperatures (200–500 K) with high accuracy and precision. Moreover, to increase ease of access to the data, a user-friendly software (H2Themobank) is developed and made publicly available.

## Background & Summary

To meet the Paris Agreement climate targets, global carbon emissions need to reach net-zero by 2050<sup>1</sup>. To achieve this the emissions from fossil fuels must be reduced and the energy mix transition to low carbon energy sources must be accelerated. Hydrogen can support this transition by replacing natural gas for domestic and industrial uses; replacing coal and natural gas for power generation; replacing fuel oil and gasoline to decarbonise transport and facilitating increased renewable energy by acting as an energy carrier to balance supply and demand. To enable hydrogen as a low carbon energy pathway, gigawatt-scale storage will be required<sup>2–5</sup>. Geological gas storage in underground salt caverns, depleted oil and gas fields and deep aquifers are proven technologies that could provide the necessary scales for hydrogen storage<sup>6–8</sup>. Hydrogen-rich town gas mixtures have been stored in geological formations since the 1970's<sup>9</sup> and currently, over 1,000,000 m<sup>3</sup> of hydrogen is stored in underground salt caverns<sup>10,11</sup>. Furthermore, several types of gas have been successfully stored in geological formations, such as natural gas, compressed air and CO<sub>2</sub>. Recent work has shown that leakage of injected and stored gas is unlikely, if rigorous standards are in place<sup>12</sup>.

The storage of gas in the subsurface as chemical energy storage, whether as natural gas or hydrogen (the working gas), requires a cushion gas (30–70% of the total gas storage volume<sup>13</sup>) to prevent brine from entering the production stream and to maintain the required reservoir pressure ensuring deliverability. As depleted gas fields are being considered as storage sites for subsurface hydrogen storage, the *in situ* gas could be used as cushion gas and hence the working and cushion gasses will be of different compositions<sup>7</sup>. For gas storage in saline aquifers, where there is very little *in situ* gas present, there is a requirement to use a cushion gas that is significantly cheaper than the working gas. Considered options for aquifer storage cushion gasses are nitrogen, due to its low price, and CO<sub>2</sub> due to its high compressibility and potential for secure storage of this greenhouse gas<sup>14–16</sup>. During the injection/production cycles, mixing of the gas components is inevitable and is determined by parameters such as mobility ratios, density differences, molecular diffusion and mechanical dispersion<sup>17</sup>. The numerical simulation of any storage scenario must confirm that the working gas can be produced with minimal cushion gas

<sup>1</sup>School of Geosciences, University of Edinburgh, Grant Institute, West Main Road, Edinburgh, EH9 3JW, UK. <sup>2</sup>TÜV SÜD National Engineering Laboratory, Scottish Enterprise Technology Park, East Kilbride, South Lanarkshire, G75 0QF, United Kingdom. <sup>3</sup>Hydrates, Flow Assurance & Phase Equilibria Research Group, Institute of GeoEnergy Engineering, School of Energy, Geoscience, Infrastructure and Society, Heriot-Watt University, Riccarton, Edinburgh, EH14 4AS, UK. ✉e-mail: [Hssnpr@ed.ac.uk](mailto:Hssnpr@ed.ac.uk); [katriona.edlmann@ed.ac.uk](mailto:katriona.edlmann@ed.ac.uk)

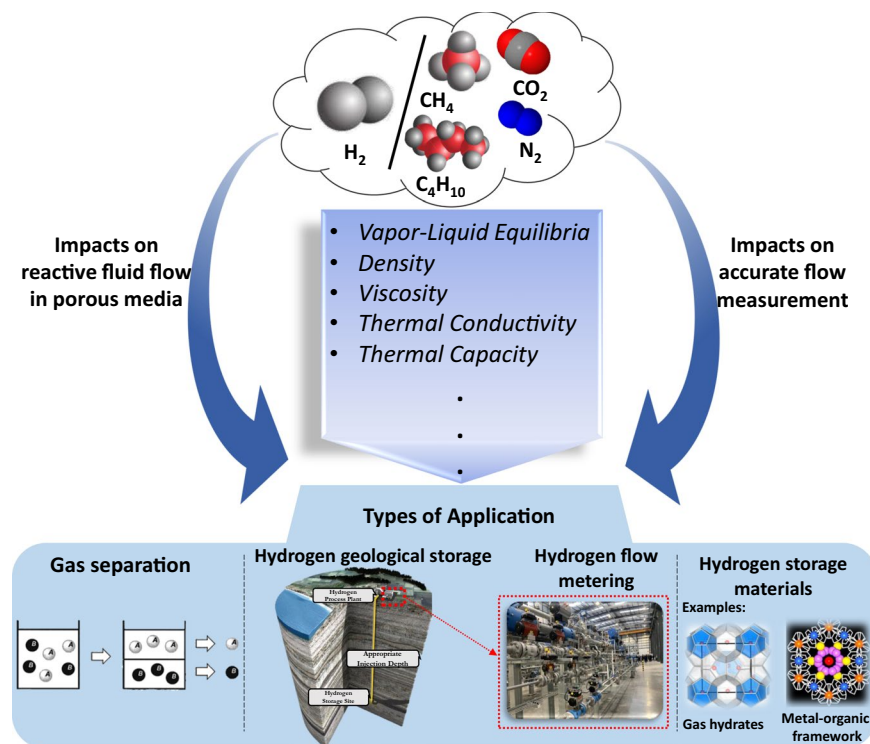


**Fig. 1** Potential applications of thermodynamic properties of hydrogen-containing streams for geological hydrogen storage, flow metering, gas separation<sup>62</sup> and other types of hydrogen storage purposes such as gas hydrates<sup>63,64</sup> or metal-organic framework<sup>65</sup>.

contamination. Therefore, if the cushion gas and working gas are of different compositions, the accurate quantification of the cushion gas/working gas mixing zone is of paramount importance. Once mixing takes place, the different gaseous components will alter the properties of the gas and introduce significant uncertainty into the expected behaviour of the injected, stored and produced gas, as shown for different gas storage applications<sup>18,19</sup>.

For gas storage modelling, accurate thermodynamic reference data for relevant fluid mixtures, which can either be directly imported into fluid flow modelling software or can be used to confirm existing reservoir engineering software outputs, is an important tool to enhance the compliance for scenario modelling results. Furthermore, the thermodynamic data for hydrogen-containing systems can enable scientists to have a deeper understanding of reactive flow through porous media during the hydrogen storage process. Another target in a hydrogen-based economy is to establish a fundamental understanding of metering technologies and the flow measurement principles behind them. In this regard, the thermo-physical properties of hydrogen mixed gases are crucial to understand and model hydrogen transportation and flow measurement processes. Thermo-physical properties of hydrogen-containing gas mixtures over a wide range of pressures and temperatures are pivotal to the design and optimisation of hydrogen production units, transportation, and storage processes (see Fig. 1).

Significant effort has been made to investigate the thermodynamic properties of hydrogen-containing mixtures systematically<sup>20–35</sup>. In addition, the phase equilibria and solubility of Hydrogen-natural gas components contained blends have been studied by researchers (see Table 1).

While the thermodynamic properties of pure hydrogen are well established<sup>36,37</sup>, published properties of gas mixtures in relation to geological hydrogen storage<sup>17,38–45</sup> do not cover the full range of additional gasses and often do not encompass the pressures and temperatures encountered within the hydrogen storage system (see Fig. 2). This data study will quantify the impacts of these additional gas components, to enable the accurate simulation of hydrogen mixed with various gases, all of which are essential for the modelling of the transportation, injection, geological storage, and production of hydrogen over multiple injection/production cycles.

## Methods

### Density and other derived thermodynamic properties using GERG-2008 Equation of State (EoS).

To efficiently design and operate the technical processes involved in gas-based energy industries, precise representation of the thermodynamic properties using an accurate EoS is essential. Here, the established and well regarded GERG-2008 EoS<sup>46</sup> was used to predict phase behaviour and density of gas mixtures relevant to hydrogen storage, covering the thermodynamic properties of gas phase, liquid phase and supercritical regions. This equation is valid over a wide range of pressures and temperatures for 21 gas components including 1-methane, 2-nitrogen, 3-carbon dioxide, 4-ethane, 5-propane, 6-n-butane, 7-iso-butane, 8-n-pentane, 9-isopentane, 10-n-hexane, 11-n-heptane, 12-n-octane, 13-hydrogen, 14-oxygen, 15-carbon monoxide, 16-water, 17-helium, 18-argon, 19-n-nonane, 20-n-decane, and 21-hydrogen sulphide. The thermodynamic properties of the fluids

No.	System: H <sub>2</sub> (1 <sup>st</sup> Component) + X (2 <sup>nd</sup> Component and beyond)	Property Type	Pressure Range (MPa)	Temperature Range (K)	x <sub>1</sub> range (1 <sup>st</sup> component liquid mole fraction)	y <sub>1</sub> range (1 <sup>st</sup> component gas mole fraction)	Reference
1	CH <sub>4</sub>	VLE/Solubility/Density/Viscosity/Compressibility/Thermal Conductivity	0.22–141.40	66.89–350.00	0.002–0.859	0.034–1.000	20–35
2	C <sub>2</sub> H <sub>6</sub>	VLE/Compressibility	0.27–562.50	83.00–283.15	0.002–0.800	0.085–1.000	26,32,71–75
3	C <sub>3</sub> H <sub>8</sub>	VLE/Compressibility	0.69–55.16	93.15–366.40	0.001–0.669	0.110–0.999	26,71,76–79
4	C <sub>4</sub> H <sub>10</sub>	VLE/Solubility	2.07–53.43	144.26–394.25	0.008–0.341	0.213–0.999	20,80–82
5	C <sub>5</sub> H <sub>12</sub>	VLE/Solubility	0.69–27.59	273.15–463.15	0.004–0.259	0.373–0.997	83,84
6	C <sub>6</sub> H <sub>14</sub>	VLE/Solubility	1.24–68.95	277.59–506.48	0.011–0.700	0.100–0.998	85–87
7	Cyclo-C <sub>6</sub> H <sub>14</sub>	VLE/Solubility	0.10–69.04	293.15–523.15	0.000–0.367	0.549–0.997	83,88–96
8	N <sub>2</sub>	VLE/Solubility/Heat Capacity/Compressibility	0.13–101.33	20.10–122.04	0.012–0.620	0.082–1.00	20,28,31,34,97–113
9	CO <sub>2</sub>	VLE/Viscosity/Density/Thermal Conductivity	0.93–191.80	219.90–298.15	0.001–0.744	0.043–0.934	108,114–118
10	H <sub>2</sub> S	Solubility	1.01–5.07	243.15–273.15	0.002–0.020	0.322–0.910	119,120
11	CO	VLE/Viscosity/Thermal Conductivity/Density	0.13–5.07	20.10–122.04	0.012–0.731	0.082–1.00	27,110,121,122
12	CH <sub>4</sub> + C <sub>2</sub> H <sub>6</sub>	VLE	0.27–562.50	83.00–283.15	0.002–0.800	0.085–1.000	72
13	C <sub>3</sub> H <sub>8</sub> + CO	VLE	0.69–20.68	88.15–348.15	0.005–0.107	0.034–0.847	79
14	CH <sub>4</sub> + CO <sub>2</sub>	VLE	6.90–27.60	227.35–258.15	0.004–0.259	0.373–0.997	84
15	CH <sub>4</sub> + CO	VLE	2.90–5.00	120.00–140.00	0.000–0.110	0.000–0.926	31
16	C <sub>5</sub> H <sub>12</sub> + CO <sub>2</sub>	VLE	6.90–27.60	273.15–323.15	0.004–0.259	0.373–0.997	84
17	N <sub>2</sub> + CO	VLE	0.003–22.80	58.15–122.04	0.012–0.930	0.082–1.00	100,109–111
18	CH <sub>4</sub> + N <sub>2</sub>	VLE	3.40–10.00	80.00–144.00	0.009–0.720	0.060–1.00	98

**Table 1.** Database of available experimental thermodynamic properties data in the literature for hydrogen-containing systems along with the temperature, pressure and composition range with respect to hydrogen for each binary/ternary system.

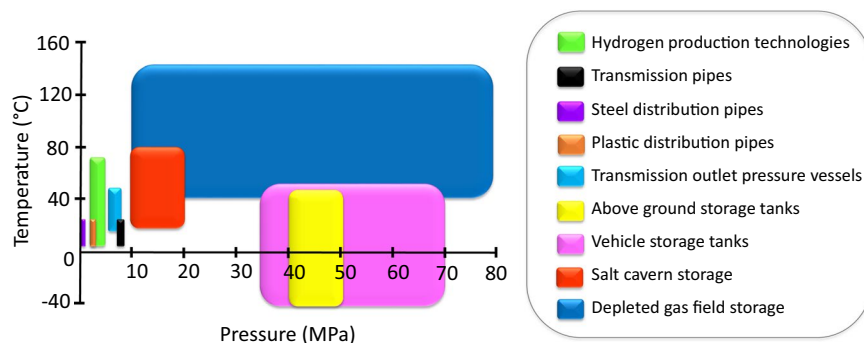


**Fig. 2** Pressure and temperature ranges for various hydrogen-based economy systems. Note that the pressure range for depleted gas fields is based on the data available for the UK only<sup>66–69</sup>.

that are predicted here at certain temperatures ( $T$ ) are based on a multi-fluid approximation using the dimensionless Helmholtz energy obtained from:

$$\alpha(\delta, \tau, \mathbf{x}) = \alpha^o(\rho, T, \mathbf{x}) + \alpha^r(\delta, \tau, \mathbf{x}) \quad (1)$$

where  $\rho$  is the mixture density and  $\mathbf{x}$  is the molar composition vector. The term  $\tau = T/T_r$  is the inverse reduced temperature, and the term  $\delta$  is the reduced density, both of which are composition-dependent i.e. they depend on the molar composition vector. The ideal-gas contribution ( $\alpha^o$ ) is related to the number of mixture components ( $N$ ), the mole fraction of each component  $i$  ( $x_i$ ), and the dimensionless Helmholtz energy of component  $i$  in the ideal-gas phase ( $\alpha_{oi}^o$ ) by:

$$\alpha^o(\rho, T, \mathbf{x}) = \sum_{i=1}^N x_i [\alpha_{oi}^o(\rho, T) + \ln x_i] \quad (2)$$

The residual part of the dimensionless Helmholtz energy ( $\alpha^r$ ) is composed of two different parts; the linear summation of the residual part of the reduced Helmholtz free energy of each component  $i$  ( $\alpha_{oi}^r$ ) and the so-called departure function ( $\Delta\alpha^r$ ) which is also a function of the mixture composition, the inverse reduced mixture temperature, and the reduced mixture density. The residual part of the dimensionless Helmholtz energy is given by:

$$\alpha^r(\delta, \tau, \mathbf{x}) = \sum_{i=1}^N x_i \alpha_{oi}^r(\delta, \tau) + \Delta \alpha^r(\delta, \tau, \mathbf{x}) \quad (3)$$

The advantage of using Helmholtz energy in the given form is that all the other thermodynamic properties can be derived analytically from terms  $\alpha^o$  and  $\alpha^r$  and their derivatives. One example is isobaric heat capacity which is given by:

$$c_p(\delta, \tau, \mathbf{x}) = R \left[ -\tau^2 (\alpha_{\tau\tau}^o + \alpha_{\tau\tau}^r) + \frac{(1 + \delta \alpha_{\delta}^r + \delta \tau \alpha_{\delta\tau}^r)^2}{1 + 2 \delta \alpha_{\delta}^r + \delta^2 \alpha_{\delta\delta}^r} \right] \quad (4)$$

where R is the gas constant. The subscriptions of  $\alpha^o$  and  $\alpha^r$  denote the order of their derivatives with respect to  $\tau$  and  $\delta$ . For example  $\alpha_{\tau\tau}^r$  denotes the second-order derivatives of  $\alpha^r$  with respect to  $\tau$ . Similarly, enthalpy (h), entropy (s), Gibbs free energy (g), pressure (P) can be obtained from:

$$P(\delta, \tau, \mathbf{x}) = RT\rho[1 + \delta \alpha_{\delta}^r] \quad (5)$$

$$h(\delta, \tau, \mathbf{x}) = RT[1 + \tau (\alpha_{\tau}^o + \alpha_{\tau}^r) + \delta \alpha_{\delta}^r] \quad (6)$$

$$s(\delta, \tau, \mathbf{x}) = R[\tau (\alpha_{\tau}^o + \alpha_{\tau}^r) - \alpha^o - \alpha^r] \quad (7)$$

$$g(\delta, \tau, \mathbf{x}) = RT[1 + \alpha_{\tau}^o + \alpha_{\tau}^r + \delta \alpha_{\delta}^r] \quad (8)$$

Other thermodynamic properties such as compression factor, internal energy, speed of sound, Joule-Thomson coefficient, etc. can be defined similarly. Kunz. *et al.*<sup>46</sup> provides comprehensive coverage of these derivatives and thermodynamic properties. In GERG-2008 EoS, terms  $\rho_r$  and  $T_r$  are calculated using quadratic mixing rules proposed by Klimeck<sup>47</sup>:

$$\frac{1}{\rho_r(\mathbf{x})} = \sum_{i=1}^N x_i^2 \frac{1}{\rho_{c,i}} + \sum_{i=1}^{N-1} \sum_{j=i+1}^N \frac{2x_i x_j}{\rho_{c,ij}} \quad (9)$$

$$T_r(\mathbf{x}) = \sum_{i=1}^N x_i^2 T_{c,i} + \sum_{i=1}^{N-1} \sum_{j=i+1}^N 2x_i x_j T_{c,ij} \quad (10)$$

where  $\rho_{c,i}$  is the critical density of component i, .. is the critical temperature of component i. The parameters for the components studied in this study are provided in figshare entry<sup>48</sup>.  $T_{c,ij}$  and  $\rho_{c,ij}$  are obtained from:

$$\frac{1}{\rho_{c,ij}} = \beta_{\nu,ij} \gamma_{\nu,ij} \frac{x_i + x_j}{\beta_{\nu,ij}^2 x_i + x_j} \cdot \frac{1}{8} \left( \frac{1}{\rho_{c,i}^{1/3}} + \frac{1}{\rho_{c,j}^{1/3}} \right)^3 \quad (11)$$

$$T_{c,ij} = \beta_{T,ij} \gamma_{T,ij} \cdot \frac{x_i + x_j}{\beta_{T,ij}^2 x_i + x_j} (T_{c,i} T_{c,j})^{1/2} \quad (12)$$

where  $\beta_{\nu,ij}$ ,  $\gamma_{\nu,ij}$ ,  $\beta_{T,ij}$ , and  $\gamma_{T,ij}$  are the four adjustable binary interaction parameters. The binary interaction parameters used for the components in this study are provided in figshare entry<sup>48</sup>.

An example of the calculated densities and isobaric heat capacity for H<sub>2</sub> + CH<sub>4</sub> mixtures over a range of pressure and temperature for various H<sub>2</sub> mole fractions is provided in Figs. 3 and 4, respectively. Plots of the other derived thermodynamic properties of H<sub>2</sub> with CH<sub>4</sub> and the thermodynamic properties of H<sub>2</sub> with CO<sub>2</sub>, N<sub>2</sub>, and the typical natural gas are presented in figshare entry<sup>48</sup>.

**Viscosity and thermal conductivity using SuperTRAPP model.** For calculating viscosity of the system we used SuperTRAPP model<sup>49</sup> that is based on the corresponding-states model. SuperTRAPP viscosity model is composed of a dilute-gas and residual contribution part, where only the latter is treated with corresponding states. The viscosity ( $\mu$ ) is a function of density and pressure and is obtained from:

$$\mu(T, \rho) = \mu^*(T) + \Delta \mu_0(T_0, \rho_0) F_{\mu}(T, \rho) \quad (13)$$

where \* refers to dilute gas and 0 refers to a reference fluid. The dilute gas viscosity is calculated using Chung *et al.*<sup>50</sup> theory which is a modification of the original model by Chapman-Enskog<sup>51</sup>. The function  $F_{\mu}$  can be obtained from:

$$F_{\mu}(T, \rho) = \sqrt{f} h^{-2/3} \sqrt{\frac{m}{m_0}} \quad (14)$$

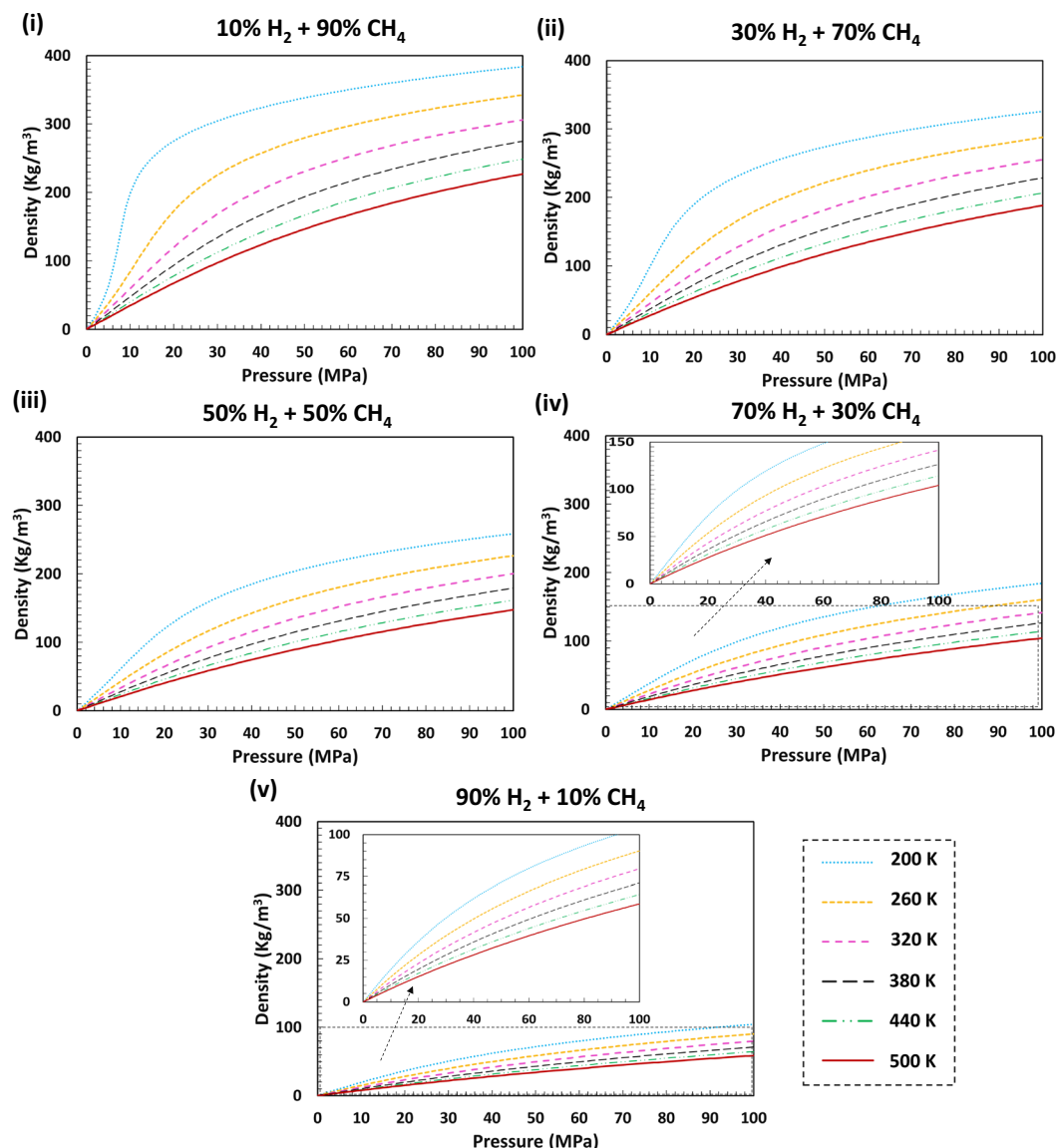


**Fig. 3** Predicted densities for different H<sub>2</sub> + CH<sub>4</sub> mixtures for various mole H<sub>2</sub> fractions over a wide range of pressures and temperatures using GERG-2008 EoS. Density values are greater in the presence of higher mole fractions of CH<sub>4</sub> in the studied systems as the density of CH<sub>4</sub> is considerably higher than that of H<sub>2</sub>. The densities increase with increasing pressure (Boyle's Law) for all isotherms and reduce with increasing temperature (Charles's Law).

where  $m$ , and  $m_0$  are the molar mass of the main fluid and the reference fluid, respectively. The terms  $f$  and  $h$  are so-called equivalent substance reducing ratios, relating the reference fluid to the studying fluid using critical parameter ratios. For a more detailed examination of the formulations used for calculating viscosity, the reader is referred to reference<sup>49</sup>. An example of calculated viscosities for H<sub>2</sub> + CH<sub>4</sub> mixtures over a range of pressures and temperatures for various H<sub>2</sub> mole fractions is provided in Fig. 5. Plots of the viscosity of H<sub>2</sub> with CO<sub>2</sub>, N<sub>2</sub>, and typical natural gas are presented in figshare entry<sup>48</sup>. To calculate the thermal conductivity of the fluids ( $\gamma$ ) we also used SuperTRAPP model<sup>49</sup>. The thermal conductivity is obtained from:

$$\gamma(T, \rho) = \gamma^{int}(T) + \overbrace{\gamma^*(T) + \gamma^r(T, \rho) + \gamma^{crit}(T, \rho)}^{trans} \quad (15)$$

This method is based on the Ely and Hanley procedure<sup>52</sup> for calculating the thermal conductivity, where the model considers the effect of collisions between molecules (translational energy transfer) ( $\gamma^{trans}$ ), and the internal motions of the molecules ( $\gamma^{int}$ , calculated using modified Eucken correlation). The former term can be further divided into three contributions i.e. dilute gas ( $\gamma^*$ ), residual ( $\gamma^r$ ) and critical enhancement ( $\gamma^{crit}$ ). We refer the reader to the article by Huber<sup>49</sup> for detailed formulation and parameters of the thermal conductivity. An example of the calculated thermal conductivities for H<sub>2</sub> + CH<sub>4</sub> mixtures over a range of pressures and temperatures for

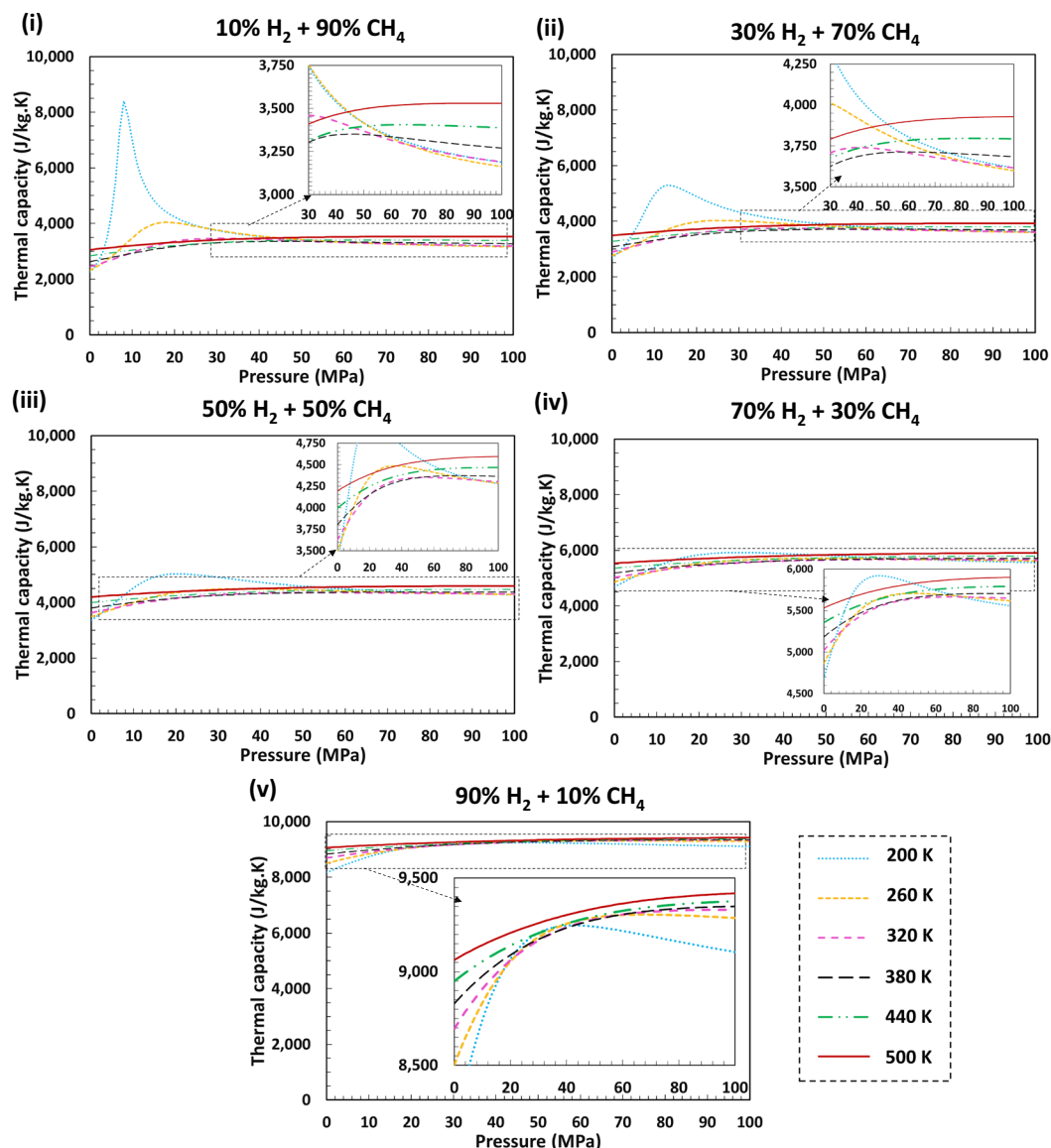


**Fig. 4** Predicted isobaric heat capacities for different  $\text{H}_2 + \text{CH}_4$  mixtures for various  $\text{H}_2$  mole fractions over a wide range of pressures and temperatures using GERG-2008 EoS. Thermal capacities have higher values for higher  $\text{H}_2$  mole fractions as the heat capacity of pure  $\text{H}_2$  is significantly higher than that of pure  $\text{CH}_4$  at temperatures and pressures above the critical point of  $\text{CH}_4$ . Generally, it can be noted that with increasing pressure, the thermal capacities increase for all temperature conditions due to increased intermolecular forces. The peaks in the graphs can be attributed to the fact that near the critical points of the components the heat capacities undergo sudden changes because of the changes in their phase. In these examples, as the temperatures and pressures are close to the critical conditions of  $\text{CH}_4$ , peaks have emerged. Reducing the mole fraction of  $\text{CH}_4$  in the system composition moves the system away from the critical point and as such the peaks reduce or do not appear in the graphs (iv and v).

various  $\text{H}_2$  mole fractions is provided in Fig. 6. The plots of thermal conductivity of  $\text{H}_2$  with  $\text{CO}_2$ ,  $\text{N}_2$ , and the typical natural gas are presented in figshare entry<sup>48</sup>.

**Vapour liquid Equilibria and isothermal flash.** For calculating phase equilibrium of the studied mixtures, we used a method established by Michelsen<sup>53</sup>. The vapour–liquid phase envelopes calculated for the system studied are provided in Fig. 7. As can be seen, some parts of two-phase envelope of the  $\text{H}_2 + \text{CO}_2$  and the  $\text{H}_2 + \text{Natural gas}$  systems occur within the pressure and temperature ranges of geological storage and as such are used in this study (temperature 200–500 K and pressure 0.01–100 MPa). For these points, we used isothermal multi-phase flash to calculate fraction and composition of gas and liquid phase. Here, we followed stability analysis by the successive substitution method which was introduced by Michelsen<sup>54</sup> to minimise the Gibbs energy of the system. This was followed by the calculation of thermodynamic properties for each phase.

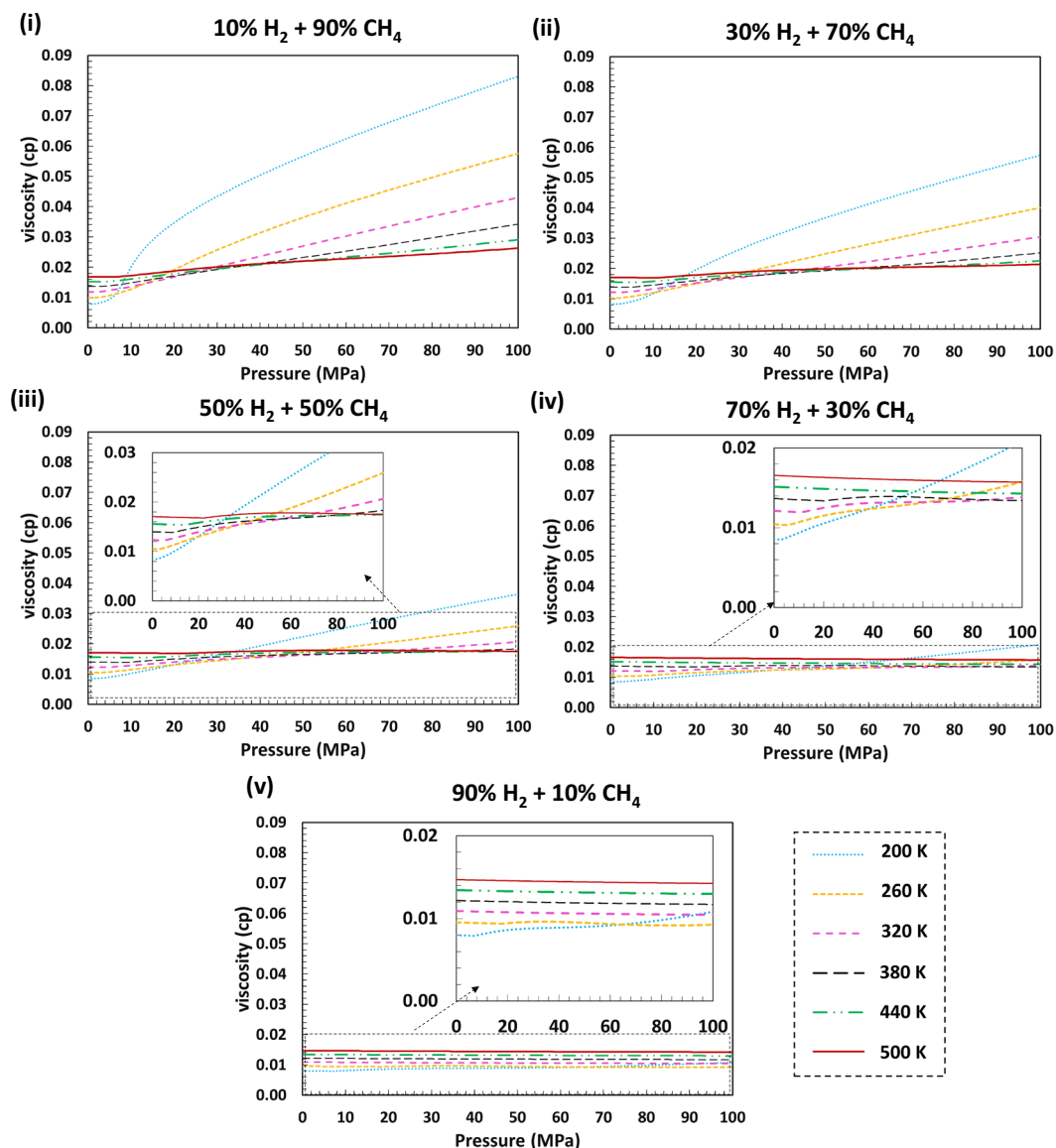


**Fig. 5** Modelled viscosity values for various  $\text{H}_2 + \text{CH}_4$  blends for different  $\text{H}_2$  mole fractions over a wide range of pressures and temperatures using GERG-2008 EoS and SuperTRAPP model. The viscosities of the mixtures are suppressed with increasing  $\text{H}_2$  mole fractions in the system as  $\text{H}_2$  has a significantly lower viscosity than  $\text{CH}_4$  due to its smaller molecule size. The viscosities of the blends increase with increasing pressure and temperature. This can be attributed to the fact that an increase in pressure or temperature increases the velocities of the random motion of molecules and as such collisions of gas molecules increase, which resists the flow of gas and increases the viscosity. The unusual behaviour of  $\text{CH}_4$ -rich blends at lower temperatures is because of their proximity to the  $\text{CH}_4$  critical point.

### Data Records

Viscosity, thermal conductivity, density, and other derived thermodynamic properties of  $\text{H}_2$  mixed with  $\text{N}_2$ ,  $\text{CO}_2$ ,  $\text{CH}_4$ , and a typical natural gas from the UK North Sea (see Table 2) is provided for temperatures between 200–500 K, pressures between 0.01–100 MPa and mole fractions of hydrogen and additional gases between 10–90% using the described method. Note that the presence of water vapour, other impurities within the natural gas composition or selecting a different natural gas composition will affect the accuracy of the properties calculated.

The calculated data is publicly available and can be obtained using the following sources:

**H2ThermoBank.** An open-source user-friendly software developed using C# code in visual studio to ease the access of data for any user.

**Excel format.** The data is uploaded to (figshare) and is publicly accessible<sup>48</sup>.

**Figure format.** Some selected data points with large steps are plotted and provided in figshare entry<sup>48</sup>.

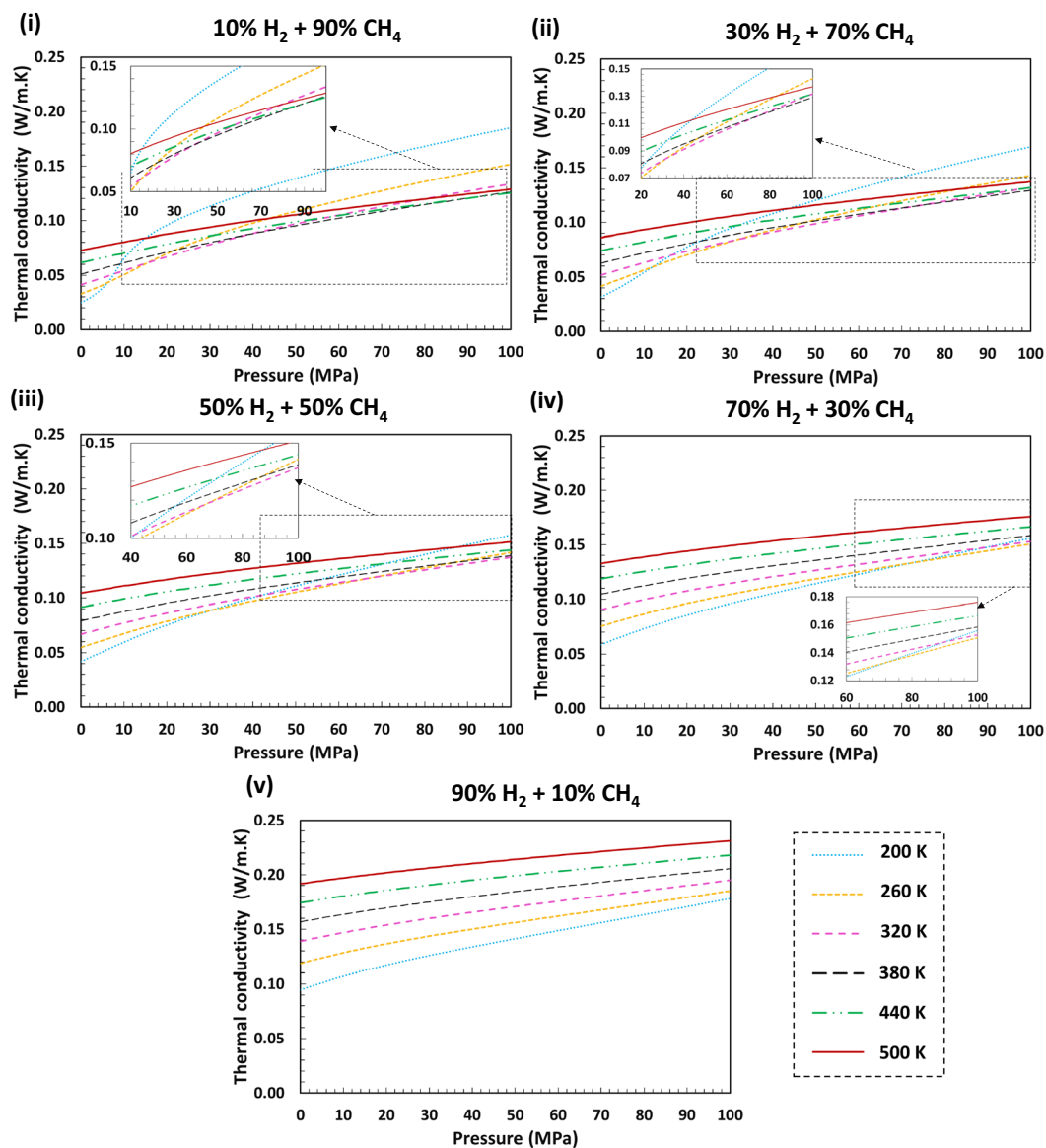


**Fig. 6** Estimated thermal conductivities for different  $\text{H}_2 + \text{CH}_4$  blends with a range of  $\text{H}_2$  mole fractions over a wide range of pressures and temperatures using GERG-2008 EoS and SuperTRAPP model. It can be inferred that for all hydrogen/methane mixtures, the thermal conductivity values increase with increasing pressure for all isotherms. Thermal conductivities also increase with temperature for high  $\text{H}_2$  mole fraction systems (above 50%). These behaviours can be attributed to the fact that increasing pressure or temperature increases the molecular motion and as such improves the conduction of heat within gas molecules. The unusual behaviour of  $\text{CH}_4$ -rich streams at lower temperatures is because of the proximity of these points to the  $\text{CH}_4$  critical point. Generally, thermal conductivity values increase with increasing hydrogen mole fractions as pure  $\text{H}_2$  has a considerably higher thermal conductivity than  $\text{CH}_4$ .

### Technical Validation

The validity of the code developed for this study is checked by comparing the calculated results for a sample natural gas with existing data in the literature. Numerous pressure and temperature points were randomly selected for this comparison. The manual validation revealed no error in the written script for this study.

The GERG-2008 EoS is valid over a wide range of temperatures, pressures, and gas compositions achieving high accuracy in the prediction of thermodynamic properties of the 21 components listed in the methods section. Although the GERG-2008 EoS has been fitted to a wide range of experimental data, for some binary mixtures only the reducing functions were used. This is because predicting a general rule for accuracy of the GERG-2008 EoS for such binary mixtures is a very challenging task as there is no experimental data available for some ranges, therefore the absolute value of error for such ranges is considered to be unknown. However, the GERG-2008 EoS has been extensively compared with available data and its validity range can be divided into three pressure/temperature ranges:



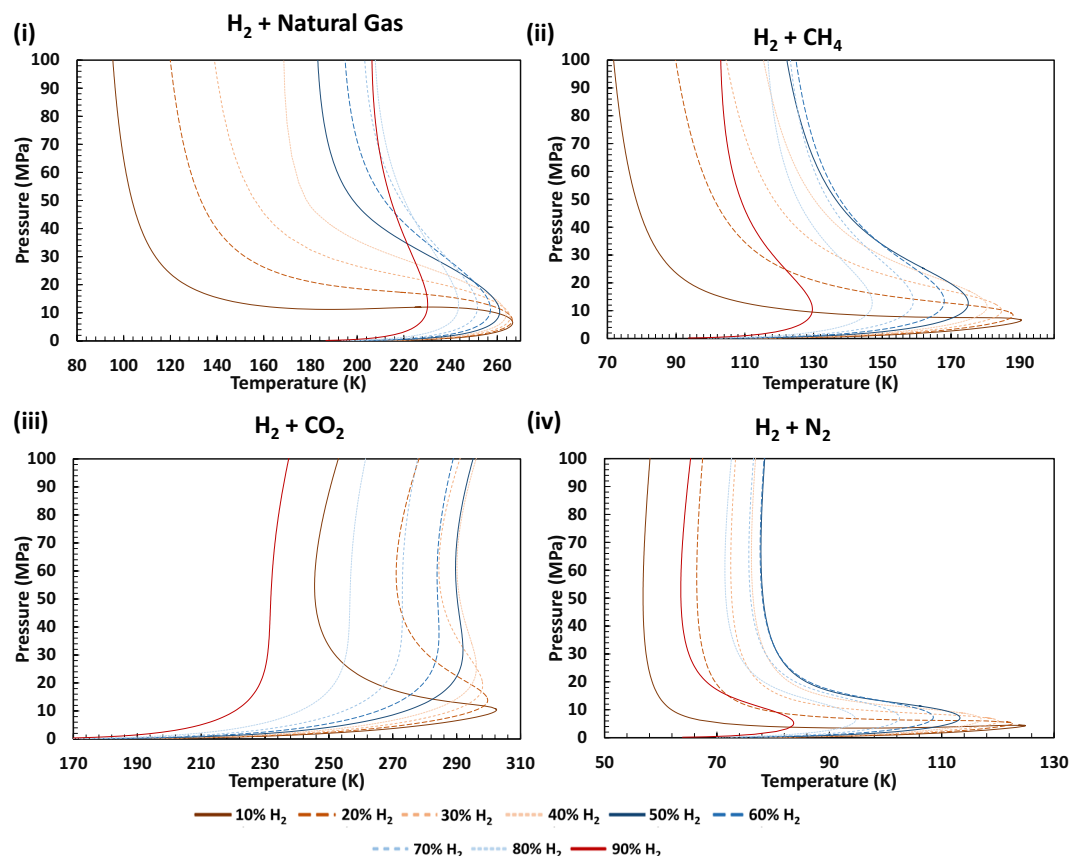


**Fig. 7** Modelled Vapour liquid Equilibria (VLE) diagrams using the developed tool in this study for various H<sub>2</sub> containing mixtures with different H<sub>2</sub> mole fractions over a wide range of pressures and temperatures. Comparing Fig. 2 with the above figure highlights that the possibility of entering into a two-phase region only exists in systems with higher CO<sub>2</sub> concentrations. We refer readers to an excellent book on thermodynamics and phase behaviour of fluids to read more details about the behaviour of mixed fluids under various pressure and temperature conditions<sup>70</sup>.

Component	Mole%
CH <sub>4</sub>	83.60
C <sub>2</sub> H <sub>4</sub>	7.48
C <sub>3</sub> H <sub>8</sub>	3.92
n-C <sub>4</sub>	0.81
i-C <sub>4</sub>	0.81
n-C <sub>5</sub>	0.15
i-C <sub>5</sub>	0.14
N <sub>2</sub>	1.95
CO <sub>2</sub>	1.14

**Table 2.** Natural gas molar composition used in this study. The composition is based on data obtained from a typical UK North Sea natural gas<sup>123</sup>.

- Normal range: which covers temperatures between 90 K and 450 K and pressures up to 35 MPa (The uncertainty of calculated density is less than 0.1% over the major part of this range)
- Extended range: which covers temperatures between 60 K and 700 K and pressures up to 70 MPa (The uncertainty of calculated density is less than 0.5% over the major part of this range)
- Extrapolated range: which covers temperatures and pressures beyond the previous range. (The uncertainty of calculated density is less than 1% over the major part of this range up to 100 MPa)

A number of studies using the same thermodynamic models have demonstrated the validity and accuracy of GERG-2008 EoS for different mixtures such as CH<sub>4</sub> mixtures<sup>55,56</sup>, CO<sub>2</sub> mixtures<sup>57,58</sup>, natural gas<sup>59,60</sup> and compressed air<sup>61</sup>.

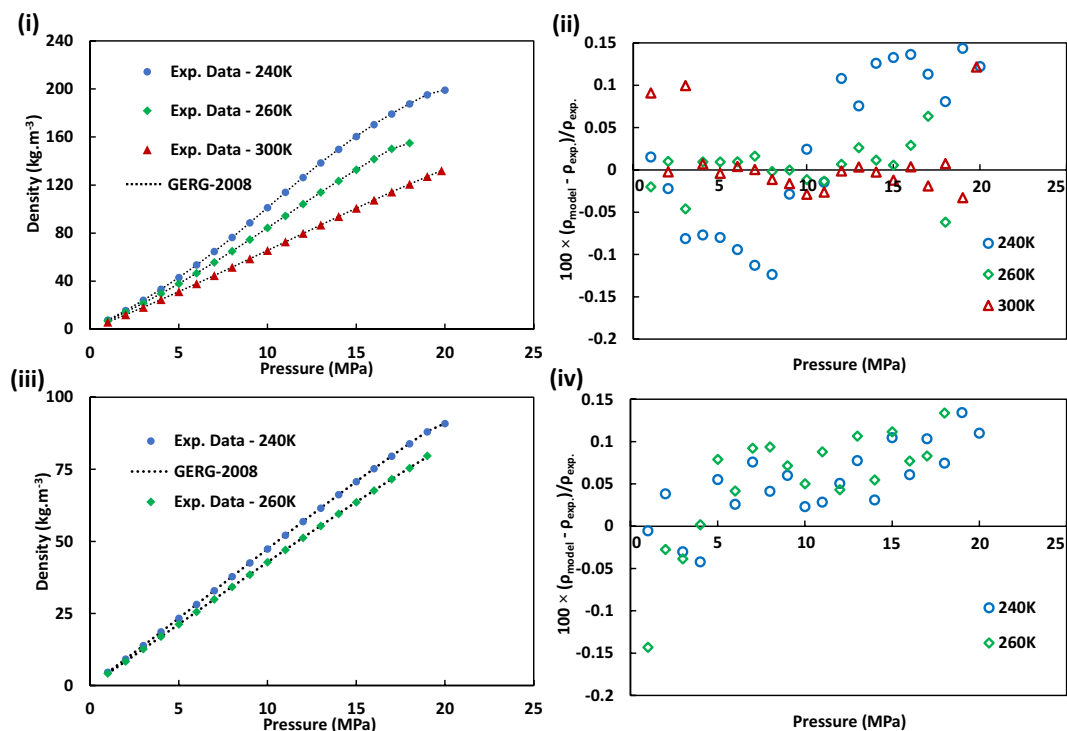


**Fig. 8** Thermodynamic modelling and experimental results of density of hydrogen/methane mixtures at a range of temperatures and pressures: i & ii are the results for a 10% $\text{H}_2$  + 90% $\text{CH}_4$  mixture and iii & iv are the results for a 50% $\text{H}_2$  + 50% $\text{CH}_4$  mixture at different pressure and temperatures. ii and iv show the relative deviations in density values predicted by GERG-2008 equation of state,  $\rho_{\text{model}}$ , from the density from the experimental ( $\rho_{\text{exp}}$ ) data<sup>23</sup> versus pressure at different temperatures. The relative expanded uncertainties in experimental density ( $k=2$ )  $U(\rho_{\text{exp}})$  for the 10% $\text{H}_2$  + 90% $\text{CH}_4$  mixture and the 50% $\text{H}_2$  + 50% $\text{CH}_4$  mixture are  $0.024 \leq U(\rho_{\text{exp}}) \leq 0.046$  and  $0.024 \leq U(\rho_{\text{exp}}) \leq 0.034$ , respectively.

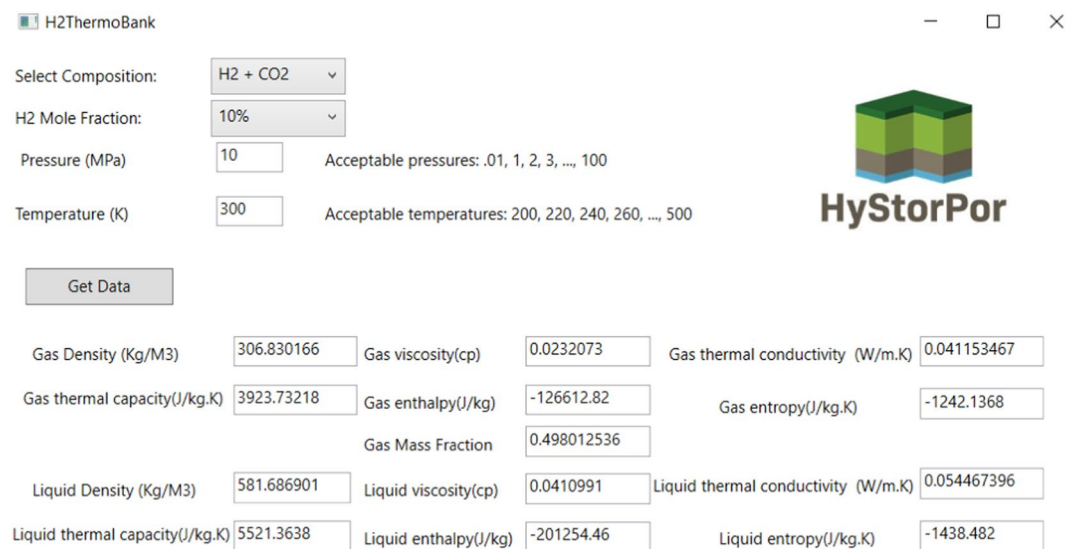


**Fig. 9** Example of graphical user interface of H2ThermoBank. Here, we chose a mixture of  $\text{CO}_2$  and  $\text{H}_2$  with 10%  $\text{H}_2$  and 90%  $\text{CO}_2$ , at 10 MPa and 300 K and clicked on the “Get Data” button. The image presents the calculated thermodynamic and transport properties of the liquid phase and the gas phase. In addition, the gas mass fraction for this mixture at the entered condition is obtained.

We have utilised published density data of hydrogen/methane blends at a range of pressure and temperature conditions to statistically analyse and assess the reliability and accuracy of the attained modelling data from the GERG-2008 EoS. Figure 8 presents the relative deviations of the predicted densities of GERG-2008 EoS from the

published hydrogen/methane blend experimental data<sup>23</sup>. The average absolute deviations (AADs) of the GERG-2008 EoS calculated data used in this study from the experimental data for the various pressures and temperatures are 0.044 for the 10% $H_2$  + 90% $CH_4$  mixture and 0.006 for the 50% $H_2$  + 50% $CH_4$  mixture. The low AAD values confirm the high accuracy of GERG-2008 EoS predictions with relatively low errors as discussed above.

The errors in viscosity and thermal conductivity estimates at various pressures, temperatures and gas compositions are uncertain due to the lack of experimental data. It is extremely time consuming and almost impossible to measure all the data required using existing laboratory methods. However, the thermal conductivity and viscosity of various compositions calculated from SuperTRAPP model have been compared with experimental data, with an error range of 0–15% reported in the literature<sup>49</sup>.

## Usage Notes

**H2ThermoBank.** A screenshot of the data bank software is provided in Fig. 9. To calculate the required data, the user initially needs to select the gas composition of the closed system. There are 4 options ( $H_2$  +  $CH_4$ ,  $H_2$  +  $N_2$ ,  $H_2$  +  $CO_2$ , and  $H_2$  + Natural gas). Following this, the  $H_2$  mole fraction in the closed system should be selected. After entering the desired pressure and temperature the “Get Data” button should be clicked to collect the data. For systems of  $H_2$  +  $CH_4$  and  $H_2$  +  $N_2$  there is only one phase exist in the covered range. It is important to note that for  $H_2$  +  $CO_2$  and  $H_2$  + Natural gas system some of the two-phase region is covered in this study (see Fig. 7). For these systems, the user will be able to get both liquid and gas properties together with the mass fraction of the gas phase.

In this study, we have utilised a newly developed tool based on the GERG-2008 EoS and SuperTRAPP model to predict different thermo-physical properties of hydrogen (e.g. density, viscosity, thermal conductivity, etc.) when mixed with other gaseous species including methane, nitrogen, carbon dioxide and a typical North Sea natural gas. The model has been applied to a wide range of pressures, temperatures, and gas mixture compositions which cover the temperature and pressure conditions experienced within the whole hydrogen-based energy system from production to storage in geological formations. The obtained results could be employed by a range of different stakeholders to effectually design and develop innovative infrastructure for the hydrogen economy.

**Excel format.** To enable easy access to the data over a wide range of temperature, pressure and concentration conditions without requiring running the abovementioned application for each point, four excel files for each of gas mixture systems are provided. Each worksheet in the excel files is allocated to a different mole fraction of hydrogen. Data provided here could be sorted and selected for a required range.

## Code availability

The code for H2ThermoBank has been made available on the H2ThermoBank GitHub page (<https://github.com/aliakbarhssnpr/H2ThermoBank>).

Received: 6 April 2020; Accepted: 15 June 2020;

Published online: 09 July 2020

## References

1. IPCC. *IPCC report Global Warming of 1.5 C: Summary for Policymakers*. (2018).
2. Taylor, J. B., Alderson, J. E. A., Kalyanam, K. M., Lyle, A. B. & Phillips, L. A. Technical and economic assessment of methods for the storage of large quantities of hydrogen. *Int. J. Hydrogen Energy* **11**, 5–22 (1986).
3. Crotagino, F., Donadei, S., Bünger, U. & Landinger, H. Large-scale hydrogen underground storage for securing future energy supplies. *In 18th World hydrogen energy conference* **78**, 37–45 (2010).
4. Panfilov, M. Underground storage of hydrogen: *in situ* self-organisation and methane generation. *Transp. porous media* **85**, 841–865 (2010).
5. Pfeiffer, W. T., Beyer, C. & Bauer, S. Hydrogen storage in a heterogeneous sandstone formation: dimensioning and induced hydraulic effects. *Pet. Geosci.* **23**, 315–326 (2017).
6. Lord, A. S. Overview of geologic storage of natural gas with an emphasis on assessing the feasibility of storing hydrogen. SAND2009-5878, Sandia Natl. Lab. Albuquerque, NM (2009).
7. Amid, A., Mignard, D. & Wilkinson, M. Seasonal storage of hydrogen in a depleted natural gas reservoir. *Int. J. Hydrogen Energy* **41**, 5549–5558 (2016).
8. Heinemann, N. *et al.* Hydrogen storage in porous geological formations—onshore play opportunities in the midland valley (Scotland, UK). *Int. J. Hydrogen Energy* **43**, 20861–20874 (2018).
9. Foh, S., Novil, M., Rockar, E. & Randolph, P. Underground hydrogen storage final report. *Inst. Gas Tech., DOE, Brookhaven Natl Lab, Upton, NY (Dec. 1979)* (1979).
10. Ozarslan, A. Large-scale hydrogen energy storage in salt caverns. *Int. J. Hydrogen Energy* **37**, 14265–14277 (2012).
11. Kruck, O., Crotagino, F., Prelicz, R. & Rudolph, T. Assessment of the potential, the actors and relevant business cases for large scale and seasonal storage of renewable electricity by hydrogen underground storage in Europe. *KBB Undergr. Technol. GmbH* (2013).
12. Alcalde, J. *et al.* Estimating geological  $CO_2$  storage security to deliver on climate mitigation. *Nat. Commun.* **9**, 1–13 (2018).
13. Flanigan, O. *Underground gas storage facilities: Design and implementation*. (Elsevier, 1995).
14. Pfeiffer, W. T. & Bauer, S. Subsurface porous media hydrogen storage—scenario development and simulation. *Energy Procedia* **76**, 565–572 (2015).
15. Oldenburg, C. M. Carbon dioxide as cushion gas for natural gas storage. *Energy & Fuels* **17**, 240–246 (2003).
16. Misra, B. R., Foh, S. E., Shikari, Y. A., Berry, R. M. & Labaune, F. The use of inert base gas in underground natural gas storage. In *SPE Gas Technology Symposium* (Society of Petroleum Engineers, 1988).
17. Feldmann, F., Hagemann, B., Ganzer, L. & Panfilov, M. Numerical simulation of hydrodynamic and gas mixing processes in underground hydrogen storages. *Environ. Earth Sci.* **75**, 1165 (2016).
18. Ma, J., Li, Q. & Kempka, T. & Kühn, M. Hydromechanical Response and Impact of Gas Mixing Behavior in Subsurface  $CH_4$  Storage with  $CO_2$ -Based Cushion Gas. *Energy & Fuels* **33**, 6527–6541 (2019).
19. Oldenburg, C. M. & Pan, L. Utilization of  $CO_2$  as cushion gas for porous media compressed air energy storage. *Greenh. Gases Sci. Technol.* **3**, 124–135 (2013).
20. Augood, D. R. The separation of HD and H2 by absorptive fractionation. *Trans Inst Chem Eng* **35**, 394–408 (1957).

21. Benham, A. L., Katz, D. L. & Williams, R. B. Phase behavior of hydrogen–light-hydrocarbon systems. *AIChE J.* **3**, 236–241 (1957).
22. Chuang, S.-Y., Chappellear, P. S. & Kobayashi, R. Viscosity of methane, hydrogen, and four mixtures of methane and hydrogen from -100. degree. C to 0. degree. C at high pressures. *J. Chem. Eng. Data* **21**, 403–411 (1976).
23. Hernández-Gómez, R., Tuma, D., Pérez, E. & Chamorro, C. R. Accurate Experimental (p,  $\rho$ , and T) Data for the Introduction of Hydrogen into the Natural Gas Grid (II): Thermodynamic Characterization of the Methane–Hydrogen Binary System from 240 to 350 K and Pressures up to 20 MPa. *J. Chem. Eng. Data* **63**, 1613–1630 (2018).
24. Machado, J. R. S., Streett, W. B. & Dieters, U. PVT measurements of hydrogen/methane mixtures at high pressures. *J. Chem. Eng. Data* **33**, 148–152 (1988).
25. Freeth, F. A. & Verschoyle, T. T. H. Physical constants of the system methane-hydrogen. *Proc. R. Soc. London. Ser. A, Contain. Pap. a Math. Phys. Character* **130**, 453–463 (1931).
26. Mihara, S., Sagara, H., Arai, Y. & Saito, S. The Compressibility Factors of Hydrogen Methane, Hydrogen Ethane and Hydrogen Propane Gaseous Mixtures. *J. Chem. Eng. Japan* **10**, 395–399 (1977).
27. Kestin, J., Ro, S. T. & Wakeham, W. A. The transport properties of binary mixtures of hydrogen with CO, CO<sub>2</sub> and CH<sub>4</sub>. *Phys. A Stat. Mech. its Appl.* **119**, 615–638 (1983).
28. Gonikberg, M. G., Fastowsky, W. G. & Gurwitsch, J. G. *The solubility of gases in liquids at low temperatures and high pressures: the solubility of hydrogen in liquid nitrogen at temperatures of 79.0-109.0 [degree] K. and pressures up to 190 atm.* (National Research Council of Canada, 1954).
29. Hong, J. H. & Kobayashi, R. Vapor-liquid equilibrium study of the hydrogen-methane system at low temperatures and elevated pressures. *J. Chem. Eng. Data* **26**, 127–131 (1981).
30. Kirk, B. S. & Ziegler, W. T. A phase-equilibrium apparatus for gas-liquid systems and the gas phase of gas-solid systems: Application to methane/hydrogen from 66.88 to 116.53 K and up to 125 atmospheres. In *Advances in Cryogenic Engineering* **10**, 160–170 (Plenum New York, 1965).
31. Kremer, H. & Knapp, H. Vapor-liquid equilibria in ternary mixtures of H<sub>2</sub>, N<sub>2</sub>, CO and CH<sub>4</sub>. *Fluid Phase Equilib.* **11**, 289–310 (1983).
32. Sagara, H., Arai, Y. & Saito, S. Vapor-liquid equilibria of binary and ternary systems containing hydrogen and light hydrocarbons. *J. Chem. Eng. Japan* **5**, 339–348 (1972).
33. Tsang, C. Y., Clancy, P., Calado, J. C. G. & Streett, W. B. Phase equilibria in the H<sub>2</sub>/CH<sub>4</sub> system at temperatures from 92.3 to 180.0 K and pressures to 140 MPa. *Chem. Eng. Commun.* **6**, 365–383 (1980).
34. Yorizane, M., Yoshimura, S., Masuoka, H. & Toyama, A. Low Temperature Vapor-Liquid Equilibria of Hydrogen-Containing Binaries. In *Proc. 1st Int. Cryog. Eng. Conf.* 57–62 (1968).
35. Yorizane, M. *et al.* Phase behavior of three hydrogen-containing ternary systems. In *Advances in Cryogenic Engineering* 654–661 (Springer, 1980).
36. Michels, A. & Goudekot, M. Compressibilities of hydrogen between 0 C and 150 C up to 3000 atmospheres. *Physica* **8**, 347–352 (1941).
37. Seward, T. M. & Franck, E. U. The system hydrogen-water up to 440 °C and 2500 bar pressure. *Berichte der Bunsengesellschaft für Phys. Chemie* **85**, 2–7 (1981).
38. Kritschewsky, I. R. & Markov, V. P. The compressibility of gas mixtures. I. The PVT data for binary and ternary mixtures of hydrogen, nitrogen and carbon dioxide. *Acta Physicochim. URSS* **12**, 59–66 (1940).
39. Kritschevskii, I. R. & Levchenko, G. T. Compressibility of gas mixtures. II. *PVT data Bin. ternary Mix. methane, nitrogen and hydrogen (in Russ. Acta Physicochim. URSS \_L4 271–278* (1941).
40. Paterson, L. The implications of fingering in underground hydrogen storage. *Int. J. Hydrogen Energy* **8**, 53–59 (1983).
41. Song, L. *et al.* Thermodynamics study of hydrogen storage materials. *J. Chem. Thermodyn.* **46**, 86–93 (2012).
42. Davarnejad, R., Rahimi, B., Baghban, S. H. N., Khansary, M. A. & Sani, A. H. Development of a thermodynamic model for hydrogen and hydrogen containing mixtures. *Fluid Phase Equilib.* **382**, 1–9 (2014).
43. Liebscher, A., Wackerl, J. & Streibel, M. Geologic Storage of Hydrogen–Fundamentals, Processing, and Projects. *Hydrog. Sci. Eng. Mater. Process. Syst. Technol.* 629–658 (2016).
44. Hagemann, B., Panfilov, M. & Ganzer, L. Multicomponent gas rising through water with dissolution in stratified porous reservoirs–Application to underground storage of H<sub>2</sub> and CO<sub>2</sub>. *J. Nat. Gas Sci. Eng.* **31**, 198–213 (2016).
45. Lim, D. *et al.* Thermodynamic stability and guest distribution of CH<sub>4</sub>/N<sub>2</sub>/CO<sub>2</sub> mixed hydrates for methane hydrate production using N<sub>2</sub>/CO<sub>2</sub> injection. *J. Chem. Thermodyn.* **106**, 16–21 (2017).
46. Kunz, O. & Wagner, W. The GERG-2008 wide-range equation of state for natural gases and other mixtures: an expansion of GERG-2004. *J. Chem. Eng. data* **57**, 3032–3091 (2012).
47. Klimeck, R. Entwicklung einer Fundamentalgleichung für Erdgase für das Gas-und Flüssigkeitsgebiet sowie das Phasengleichgewicht. (2000).
48. Hassanpouryouzband, A., Joonaki, E., Edlmann, K., Heinemann, N. & Yang, J. Thermodynamic and Transport Properties of Hydrogen Containing Streams: Data sets. *figshare* <https://doi.org/10.6084/m9.figshare.12063297> (2020).
49. Huber, M. L. *Models for Viscosity, Thermal Conductivity, and Surface Tension of Selected Pure Fluids as Implemented in REFPROP v10.0.* (2018).
50. Chung, T. H., Ajlan, M., Lee, L. L. & Starling, K. E. Generalized multiparameter correlation for nonpolar and polar fluid transport properties. *Ind. Eng. Chem. Res.* **27**, 671–679 (1988).
51. Lohrenz, J., Bray, B. G. & Clark, C. R. Calculating Viscosities of Reservoir Fluids From Their Compositions. *J. Pet. Technol.* **16**, 1171–1176 (1964).
52. Ely, J. F. & Hanley, H. J. M. Prediction of transport properties. 2. Thermal conductivity of pure fluids and mixtures. *Ind. Eng. Chem. Fundam.* **22**, 90–97 (1983).
53. Michelsen, M. L. Calculation of phase envelopes and critical points for multicomponent mixtures. *Fluid Phase Equilib.* **4**, 1–10 (1980).
54. Michelsen, M. L. The isothermal flash problem. Part I. Stability. *Fluid Phase Equilib.* **9**, 1–19 (1982).
55. Rowland, D., Hughes, T. J. & May, E. F. Extending the GERG-2008 equation of state: Improved departure function and interaction parameters for (methane+ butane). *J. Chem. Thermodyn.* **97**, 206–213 (2016).
56. Hernández-Gómez, R., Tuma, D., Villamañán, M. A., Mondéjar, M. E. & Chamorro, C. R. Accurate thermodynamic characterization of a synthetic coal mine methane mixture. *J. Chem. Thermodyn.* **68**, 253–259 (2014).
57. Elshahomi, A. *et al.* Decompression wave speed in CO<sub>2</sub> mixtures: CFD modelling with the GERG-2008 equation of state. *Appl. Energy* **140**, 20–32 (2015).
58. Gernert, J. & Span, R. EOS–CG: A Helmholtz energy mixture model for humid gases and CCS mixtures. *J. Chem. Thermodyn.* **93**, 274–293 (2016).
59. Dauber, F. & Span, R. Modelling liquefied-natural-gas processes using highly accurate property models. *Appl. Energy* **97**, 822–827 (2012).
60. Lentner, R., Richter, M., Kleinrahm, R. & Span, R. Density measurements of liquefied natural gas (LNG) over the temperature range from (105 to 135) K at pressures up to 8.9 MPa. *J. Chem. Thermodyn.* **112**, 68–76 (2017).
61. Budt, M., Wolf, D., Span, R. & Yan, J. A review on compressed air energy storage: Basic principles, past milestones and recent developments. *Appl. Energy* **170**, 250–268 (2016).
62. Hassanpouryouzband, A. *et al.* Insights into CO<sub>2</sub> Capture by Flue Gas Hydrate Formation: Gas Composition Evolution in Systems Containing Gas Hydrates and Gas Mixtures at Stable Pressures. *ACS Sustain. Chem. Eng.* **6**, 5732–5736 (2018).

63. Struzhkin, V. V., Militzer, B., Mao, W. L., Mao, H. K. & Hemley, R. J. Hydrogen storage in molecular clathrates. *Chem. Rev.* **107**, 4133–4151 (2007).
64. Hassanpouryouzband, A. *et al.* An Experimental Investigation on the Kinetics of Integrated Methane Recovery and CO<sub>2</sub> Sequestration by Injection of Flue Gas into Permafrost Methane Hydrate Reservoirs. *Sci. Rep.* **9**, 1–9 (2019).
65. Murray, L. J., Dincă, M. & Long, J. R. Hydrogen storage in metal–organic frameworks. *Chem. Soc. Rev.* **38**, 1294–1314 (2009).
66. Gluyas, J. G. & Hichens, H. M. United Kingdom oil and gas fields: commemorative millennium volume. In (Geological Society of London, 2003).
67. Dodds, P. E. & Demoullin, S. Conversion of the UK gas system to transport hydrogen. *Int. J. Hydrogen Energy* **38**, 7189–7200 (2013).
68. Bünger, U., Michalski, J., Crotogino, F. & Kruck, O. Large-scale underground storage of hydrogen for the grid integration of renewable energy and other applications. In *Compendium of Hydrogen Energy* 133–163 (Elsevier, 2016).
69. Nash, D., Aklil, D., Johnson, E., Gazey, R. & Ortisi, V. Hydrogen storage: compressed gas. (2012).
70. Danesh, A. *PVT and phase behaviour of petroleum reservoir fluids*. (Elsevier, 1998).
71. Williams, R. B. & Katz, D. L. Vapor-Liquid Equilibria in Binary Systems. Hydrogen with Ethylene, Ethane, Propylene, and Propane. *Ind. Eng. Chem.* **46**, 2512–2520 (1954).
72. Cohen, A. E., Hipkin, H. G. & Koppany, C. R. Experimental Vapor-Liquid Equilibrium Data for Hydrogen-Ethane and Hydrogen-Methane-Ethane. In *Chemical Engineering Progress Symposium Series* **63**, 10–17 (1967).
73. Heintz, A. & Streett, W. B. Phase equilibria in the hydrogen/ethane system at temperatures from 92.5 to 280.1 K and pressures to 560 MPa. *J. Chem. Eng. Data* **27**, 465–469 (1982).
74. Hiza, M. J., Heck, C. K. & Kidnay, A. J. Liquid-vapor and solid-vapor equilibrium in the system hydrogen-ethane. In *Advances in Cryogenic Engineering* 343–356 (Springer, 1995).
75. Levitskaya, E. & Pryannikov, K. Equilibrium between liquid and vapor in the binary system of hydrogen and ethane. *Zh. Tekh. Fiz.* **9**, 1849–1853 (1939).
76. Bol'shakov, P. E. & Linshits, L. R. Phase equilibria in liquid-gas systems at high pressures. *Tr. GIAP* **3**, 18–27 (1954).
77. Burriss, W. L., Hsu, N. T., Reamer, H. H. & Sage, B. H. Phase behavior of the hydrogen-propane system. *Ind. Eng. Chem.* **45**, 210–213 (1953).
78. Trust, D. B. The Heterogeneous Phase Behavior Of The Hydrogen-Propane, Carbon-Monoxide-Propane And Hydrogen-Carbon-Monoxide-Propane Systems. (1969).
79. Trust, D. B. & Kurata, F. Vapor-liquid phase behavior of the hydrogen-propane and hydrogen-carbon monoxide-propane systems. *AIChE J.* **17**, 86–91 (1971).
80. Aroyan, H. J. & Katz, D. L. Low Temperature Vapor-Liquid Equilibria in Hydrogen-n-Butane System. *Ind. Eng. Chem.* **43**, 185–189 (1951).
81. Klink, A. E., Cheh, H. Y. & Amick, E. H. Jr. The vapor-liquid equilibrium of the hydrogen—n-butane system at elevated pressures. *AIChE J.* **21**, 1142–1148 (1975).
82. Nelson, E. E. & Bonnell, W. S. Solubility of Hydrogen in n-Butane. *Ind. Eng. Chem.* **35**, 204–206 (1943).
83. Connolly, J. F. & Kandalic, G. A. Gas solubilities, vapor-liquid equilibria, and partial molal volumes in some hydrogen-hydrocarbon systems. *J. Chem. Eng. Data* **31**, 396–406 (1986).
84. Freitag, N. P. & Robinson, D. B. Equilibrium phase properties of the hydrogen—methane—carbon dioxide, hydrogen—carbon dioxide—n-pentane and hydrogen—n-pentane systems. *Fluid Phase Equilib.* **31**, 183–201 (1986).
85. Fu, M.-S. & Tan, C.-S. Solubility of hydrogen in a mixture of n-hexane and dicyclopentadiene from 313 to 363 K and from 2.0 to 5.5 MPa. *Fluid Phase Equilib.* **93**, 233–247 (1994).
86. Gao, W., Robinson, R. L. & Gasem, K. A. M. Solubilities of Hydrogen in Hexane and of Carbon Monoxide in Cyclohexane at Temperatures from 344.3 to 410.9 K and Pressures to 15 MPa. *J. Chem. Eng. Data* **46**, 609–612 (2001).
87. Nichols, W. B., Reamer, H. H. & Sage, B. H. Volumetric and phase behavior in the hydrogen—n-hexane system. *AIChE J.* **3**, 262–267 (1957).
88. Peramanu, S. & Pruden, B. B. Solubility study for the purification of hydrogen from high pressure hydrocracker off-gas by an absorption-stripping process. *Can. J. Chem. Eng.* **75**, 535–543 (1997).
89. Brainard, A. J. & Williams, B. Vapor-liquid equilibrium for the system hydrogen—benzene—cyclohexane—n-hexane. *AIChE J.* **13**, 60–69 (1967).
90. Ipatiev, V. V. & Levin, M. I. Equilibrium between liquid and gas at high pressures and temperatures. I. Solubility of hydrogen in individual hydrocarbons of the aromatic and the naphthenic series. *Zh. Fiz. Khim.* **6**, 632–639 (1935).
91. Thompson, R. E. & Edmister, W. C. Vapor-liquid equilibria in hydrogen-benzene and hydrogen-cyclohexane mixtures. *AIChE J.* **11**, 457–461 (1965).
92. Herskowitz, M., Wisniak, J. & Skladman, L. Hydrogen solubility in organic liquids. *J. Chem. Eng. Data* **28**, 164–166 (1983).
93. Berty, T. E., Reamer, H. H. & Sage, B. H. Phase Behavior in the Hydrogen-Cyclohexane System. *J. Chem. Eng. Data* **11**, 25–30 (1966).
94. Dymond, J. H. Solubility of a Series of Gases in Cyclohexane and Dimethylsulfoxide. *J. Phys. Chem.* **71**, 1829–1831 (1967).
95. Krichevskii, I. R. & Sorina, G. A. Phase and Volume Relations in Liquid-Gas Systems Under High Pressure. 6. The Cyclohexane-Hydrogen System. *Zhurnal Fiz. Khimii* **32**, 2080–2086 (1958).
96. Ronze, D., Fongarland, P., Pitault, I. & Forissier, M. Hydrogen solubility in straight run gasoil. *Chem. Eng. Sci.* **57**, 547–553 (2002).
97. Omar, M. H. & Dokoupil, Z. Some supplementary measurements on the vapour-liquid equilibrium of the system hydrogen-nitrogen at temperatures higher than the triple point of nitrogen. *Physica* **28**, 33–43 (1962).
98. Shtekkel, F. A. & Tsin, N. M. Determination of the composition diagram for the liquid-gas system methane-nitrogen-hydrogen. *Zhurnal Khimicheskoi Promyshlennosti* **16**, 24–28 (1939).
99. Streett, W. B. & Calado, J. C. G. Liquid-vapour equilibrium for hydrogen + nitrogen at temperatures from 63 to 110 K and pressures to 57 MPa. *J. Chem. Thermodyn.* **10**, 1089–1100 (1978).
100. Verschoyle, T. T. H. The ternary system carbon monoxide-nitrogen-hydrogen and the component binary systems between temperatures of -185° and -215°C., and between pressures of 0 and 225 atm. *Philos. Trans. R. Soc. London. Ser. A, Contain. Pap. a Math. or Phys. Character* **230**, 189–220 (1931).
101. Yorizane, M., Yoshimura, S., Masuoka, H. & Naka, T. Measurement and prediction of the vapor-liquid equilibrium relation at low temperature and high pressure for the hydrogen-nitrogen system. *Kagaku Kogaku* **35**, 691–693 (1971).
102. Bartlett, E. P. The compressibility isotherms of hydrogen, nitrogen and mixtures of these gases at 0 and pressures to 1000 atmospheres. A correction. *J. Am. Chem. Soc.* **49**, 1955–1957 (1927).
103. Bartlett, E. P. The compressibility isotherms of hydrogen, nitrogen and mixtures of these gases at 0° and pressures to 1000 atmospheres. *J. Am. Chem. Soc.* **49**, 687–701 (1927).
104. Bennett, C. O. & Dodge, B. F. Compressibilities of mixtures of hydrogen and nitrogen above 1000 atmospheres. *Ind. Eng. Chem.* **44**, 180–185 (1952).
105. Sage, B. H., Olds, R. H. & Lacey, W. N. Two gaseous mixtures containing hydrogen and nitrogen. *Ind. Eng. Chem.* **40**, 1453–1459 (1948).
106. Verschoyle, T. T. H. Isotherms of hydrogen, of nitrogen, and of hydrogen-nitrogen mixtures, at 0° and 20°C., up to a pressure of 200 atmospheres. *Proc. R. Soc. London. Ser. A, Contain. Pap. a Math. Phys. Character* **111**, 552–576 (1926).

107. Wiebe, R. & Gaddy, V. L. The compressibilities of hydrogen and of four mixtures of hydrogen and nitrogen at 0, 25, 50, 100, 200 and 300 and to 1000 atmospheres. *J. Am. Chem. Soc.* **60**, 2300–2303 (1938).
108. Yorizane, M. Determination of vapor-liquid equilibrium data at high pressure and low temperature. *Asahi Garasu Kogyo Gijutsu Shoreikai Kenkyu Hokoku* **18**, 61–76 (1971).
109. Akers, W. W. & Eubanks, L. S. Vapor-liquid equilibria in the system hydrogen-nitrogen-carbon monoxide. In *Advances in Cryogenic Engineering* 275–293 (Springer, 1960).
110. Dokoupil, Z., Van Soest, G. & Swenker, M. D. P. On the equilibrium between the solid phase and the gas phase of the systems hydrogen-nitrogen, hydrogen-carbon monoxide and hydrogen-nitrogen-carbon monoxide. *Appl. Sci. Res. Sect. A* **5**, 182–240 (1955).
111. Eubanks, L. S. Vapor-Liquid equilibria in the system Hydrogen-Nitrogen-Carbon monoxide. (1957).
112. Knapp, H., Schmölling, K. & Neumann, A. Measurement of the molal heat capacity of H<sub>2</sub>/N<sub>2</sub> mixtures. *Cryogenics (Guildf)*. **16**, 231–237 (1976).
113. Maimoni, A. Liquid-vapor equilibria in the hydrogen-nitrogen and deuterium-nitrogen systems. *AIChE J.* **7**, 371–375 (1961).
114. Spano, J. O., Heck, C. K. & Barrick, P. L. Liquid-vapor equilibria of the hydrogen-carbon dioxide system. *J. Chem. Eng. Data* **13**, 168–171 (1968).
115. Bezahehtak, K., Combes, G. B., Dehghani, F., Foster, N. R. & Tomasko, D. L. Vapor– Liquid equilibrium for binary systems of carbon dioxide+ methanol, hydrogen+ methanol, and hydrogen+ carbon dioxide at high pressures. *J. Chem. Eng. Data* **47**, 161–168 (2002).
116. Kaminishi, G. & Toriumi, T. Gas-liquid equilibrium under high pressures. VI. Vapor-liquid phase equilibrium in the CO<sub>2</sub>-H<sub>2</sub>, CO<sub>2</sub>-N<sub>2</sub>, and CO<sub>2</sub>-O<sub>2</sub> systems. *Kogyo Kagaku Zasshi* **69**, 175–178 (1966).
117. Ke, J., Han, B., George, M. W., Yan, H. & Poliakoff, M. How does the critical point change during a chemical reaction in supercritical fluids? A study of the hydroformylation of propene in supercritical CO<sub>2</sub>. *J. Am. Chem. Soc.* **123**, 3661–3670 (2001).
118. Yorizane, M., Yoshimura, S. & Masuoka, H. Vapor liquid equilibrium at high pressure (N<sub>2</sub>-CO<sub>2</sub>, H<sub>2</sub>-CO<sub>2</sub> system). *Kagaku Kagaku* **34**, 953–957 (1970).
119. Yorizane, M., Sadamoto, S., Masuoka, H. & Eto, Y. Solubility of gases in methanol at high pressures. *Kogyo Kagaku Zasshi* **72**, 2174–2177 (1969).
120. Qian, J.-W., Jaubert, J.-N. & Privat, R. Phase equilibria in hydrogen-containing binary systems modeled with the Peng–Robinson equation of state and temperature-dependent binary interaction parameters calculated through a group-contribution method. *J. Supercrit. Fluids* **75**, 58–71 (2013).
121. Scott, G. A. The isotherms of hydrogen, carbon monoxide and their mixtures. *Proc. R. Soc. London. Ser. A, Contain. Pap. a Math. Phys. Character* **125**, 330–344 (1929).
122. Townsend, D. T. A. & Bhatt, L. A. Isotherms of hydrogen, carbon monoxide and their mixtures. *Proc. R. Soc. London. Ser. A, Contain. Pap. a Math. Phys. Character* **134**, 502–512 (1931).
123. NLOG. Gas Properties, <https://www.nlog.nl/en/gas-properties> (2006).

## Acknowledgements

This research was supported by funding from the Engineering and Physical Sciences Research Council (EPSRC) [grant number EP/S027815/1]. Edris Joonaki thanks the Flow Programme project related to Hydrogen metrology sponsored by the UK Department for Business, Energy and Industrial Strategy (BEIS).

## Author contributions

Aliakbar Hassanpouryouzband conceived the idea presented in the manuscript, undertook the modelling study and wrote the manuscript. Edris Joonaki conducted the literature review, undertook the uncertainty/error analysis, evaluated GERG-2008 EoS respect to the experimental data, and contributed to the writing of the manuscript. Katriona Edlmann contributed to the writing of the manuscript and supervised the research. Niklas Heinemann contributed to the writing of the manuscript and edited the final manuscript. Jinhai edited the final manuscript and supervised the modelling study. All the authors discussed the results and contributed to the final manuscript.

## Competing interests

The authors declare no competing interests.

## Additional information

**Correspondence** and requests for materials should be addressed to A.H. or K.E.

**Reprints and permissions information** is available at [www.nature.com/reprints](http://www.nature.com/reprints).

**Publisher's note** Springer Nature remains neutral with regard to jurisdictional claims in published maps and institutional affiliations.



**Open Access** This article is licensed under a Creative Commons Attribution 4.0 International License, which permits use, sharing, adaptation, distribution and reproduction in any medium or format, as long as you give appropriate credit to the original author(s) and the source, provide a link to the Creative Commons license, and indicate if changes were made. The images or other third party material in this article are included in the article's Creative Commons license, unless indicated otherwise in a credit line to the material. If material is not included in the article's Creative Commons license and your intended use is not permitted by statutory regulation or exceeds the permitted use, you will need to obtain permission directly from the copyright holder. To view a copy of this license, visit <http://creativecommons.org/licenses/by/4.0/>.

The Creative Commons Public Domain Dedication waiver <http://creativecommons.org/publicdomain/zero/1.0/> applies to the metadata files associated with this article.

© The Author(s) 2020